PCCP

Accepted Manuscript

ROYAL SOCIETY OF CHEMISTRY

www.rsc.org/pccp

Catalytic effect of water, water dimer and water trimer on the $H_2S + {}^3O_2$ formations from the HO_2 + HS reaction in tropospheric conditions†

Tianlei Zhang[a,*], Chen Yang[a], Xukai Feng[a], Jiaxin Kang[a], Liang Song[a], Yousong Lu[a], Zhiyin Wang[a], Qiong Xu[a], Wenliang Wang[b,*], Zhuqing Wang[c]

[a] *Shaanxi Province Key Laboratory of Catalytic Fundamental & Application, School of Chemical & Environment Science, Shaanxi University of Technology, Hanzhong, Shaanxi 723001, China*

[b] *Key Laboratory for Macromolecular Science of Shaanxi Province, School of Chemistry & Chemical Engineering, Shaanxi Normal University, Xi'an, Shaanxi 710062, China*

[c] *Shandong Provincial Key Laboratory of Ocean Environment Monitoring Technology, Shandong Academy of Sciences Institute of Oceanographic Instrumentation, Qingdao 266001, China.*

Abstract

In this article, the reaction mechanisms of the $H_2S + {}^3O_2$ formations from the HO_2 + HS reaction without and with catalyst *X* (*X* = H_2O, $(H_2O)_2$ and $(H_2O)_3$) have been investigated theoretically at the CCSD(T)/6-311++G(3df,2pd)//B3LYP/6-311+G(2df,2p) level of theory, coupled with rate constant calculations by using conventional transition state theory. Our results show that, incorporation of the catalyst *X* (*X* = H_2O, $(H_2O)_2$ and $(H_2O)_3$) into the channel of $H_2S + {}^3O_2$ formations, the reactions between SH radical and $HO_2\cdots(H_2O)_n$ (*n* = 1-3) complexes are more favorable than the corresponding reactions of HO_2 radical with $HS\cdots(H_2O)_n$ (*n* = 1-3) complexes due to the lower barrier of the former reactions and the larger concentrations of $HO_2\cdots(H_2O)_n$ (*n* = 1-3) complexes. Meanwhile, the catalytic effect of water, water dimer and water trimer is mainly taken from the contribution of a single water vapor, due to the total effective rate constant of $HO_2\cdots H_2O$ + HS and $H_2O\cdots HO_2$ + HS reactions was respectively larger by 7-9, 9-12 orders of magnitude than that of SH + $HO_2\cdots(H_2O)_2$ and SH + $HO_2\cdots(H_2O)_3$ reactions. Besides, the enhancement factor of water vapor is only 0.37% at 240 K, while at high temperature, such as 425 K, the positive water vapor effect enhances up to 38.00%, showing at high temperatures the positive water effect is obvious under atmospheric conditions. Overall, the results will give a new example on how water and water clusters catalyzed the gas phase reactions under atmospheric conditions.

Key words: HO_2; Dual level direct dynamics; Water Effect; Tropospheric Conditions

*Corresponding authors. Tel: +86-0916-2641083, Fax: +86-0916-2641083. e-mail: ztianlei88@163.com (T. L Zhang); wlwang@snut.edu.cn (W. L. Wang).

†Electronic supplementary information (ESI) available: Geometrical parameters for the reaction of HO_2 + HS without and with catalyst *X* ((*X* = H_2O, $(H_2O)_3$ and $(H_2O)_3$)) optimized at the CCSD(T)/6-311++G(3df, 2pd)//B3LYP/6-311+G(2df, 2p) level of theory respectively describes in Figures S1, S3, S4 and S6; Figures S2 shows the schematic energy diagram of the naked HO_2 + HS reaction energies; Zero point energy (ZPE/(kcal·mol^{-1})), relative energies (ΔE and $\Delta(E+ZPE)$/(kcal·mol^{-1})), enthalpies ($\Delta H(298)$/(kcal·mol^{-1})), and free energies ($\Delta G(298)$/(kcal·mol^{-1})) for the HO_2 + HS reaction without and with catalyst *X* ((*X* = H_2O, $(H_2O)_3$ is listed in Table S1, S4, S7 and S12, respectively; Zero point energy (ZPE/(kcal·mol^{-1})), entropies (S/ (cal·mol^{-1}·K^{-1})), relative energies (ΔE and Δ(E+ZPE)/(kcal·mol^{-1})), enthalpies (ΔH(298)/(kcal·mol^{-1})), and free energies (ΔG(298)/(kcal·mol^{-1})) for the binary complexes ($H_2O\cdots HO_2$, $HO_2\cdots H_2O$, $HS\cdots H_2O$, $HS\cdots H_2O$, and $H_2O\cdots H_2O$), trinary complexes ($HO_2\cdots(H_2O)_2$, $HO_2\cdots(H_2O)_2$a, $HO_2\cdots(H_2O)_2$b, $HS\cdots(H_2O)_2$, $HS\cdots(H_2O)_2$a and $(H_2O)_2$) is listed in Table S3 and S6, respectively; Figure S5 displays the schematic energy diagrams of water dimer-assisted the channel of $H_2S + {}^3O_2$ formations occurring through $HO_2\cdots(H_2O)_2$b + HS; Rate constants (cm^3·molecules^{-1}·s^{-1}) for main reaction of the HO_2 + HS reaction without and with catalyst *X* ((*X* = H_2O, $(H_2O)_3$ and $(H_2O)_3$)) within the temperature range of 240.0-425.0 K displays in Tables S2, S5, S9, S10, and S14.

1. Introduction

Sulfur usually occurs in many hydrocarbon fuels, such as coals, petroleum fuels, and natural gases as well as biomass and wastes, [1-3] and the organic sulfur includes mainly sulfides, disulfides, thiols, thiophenes, and cyclic sulfides. These sulfur forms undergo transformation during thermal processing, such as pyrolysis, gasification, liquefaction, and combustion, which result in release of various types of sulfur compounds into the environment.[3-6] The HS radical is not only a key intermediate in sulfur transformation during thermal processing of coal, but also an important intermediate in the atmospheric chemistry of hydrogen sulfide.[7] It is clear that the HS radical is a key species in sulfur cycle. There was report that the major tropospheric process that removes H_2S is the reaction with OH, producing HS and H_2O.[8] Almost all the HS is oxidized generated to SO_2 or SO_3 finally contributes to acid rain, via the reactions with atoms or molecules, such as Cl,[9, 10] NO,[11] NO_2,[12] N_2O,[13] O_3, [14]O_2,[15] and CH_3,[16]:

$$HS + Cl \rightarrow HSCl \text{ or } HCl + S \quad (1)$$

$$HS + NO \rightarrow HSN{=}O \quad (2)$$

$$HS + NO_2 \rightarrow HSO + NO \quad (3)$$

$$HS + N_2O \rightarrow N_2 + HSO \quad (4)$$

$$HS + O_3 \rightarrow HSO + O_2 \quad (5)$$

$$HS + O_2 \rightarrow OH + SO \quad (6)$$

$$HS + CH_3 \rightarrow CH_4 + S \text{ or } CH_3SH \quad (7)$$

HO_2 radical is not only an important free radical in atmospheric chemistry, but also a key intermediates in hydrocarbon fuel combustion, atmospheric photolysis cycle and biochemical processes. Previous study has revealed that HS can also react with HO_2 radical:[19]

$$HO_2 + HS \rightarrow H_2S + {}^3O_2 \quad (8)$$

Obviously, the reaction supply a reverse path between H_2S and HS in the sulfur cycle. So, the reaction between HO_2 and HS was investigated theoretically in our recent report,[17] and the channel of the $H_2S + {}^3O_2$ formations (Eq (8)) on the triplet potential energy surface was identified as the most favorable channel. However, this effort has only focused on the non-catalytic process of the HO_2 + HS reaction.

Water is of great abundance in the Earth's atmosphere and its monomer can form hydrogen bonded complexes[18] with other radical or molecules such as HO_2

radical,[19-21] OH radical,[22-24] formic acid,[25] nitric acid,[26] acetaldehyde,[27] acetone,[28] HOCl,[24] glyoxal,[29] DMS,[30] and proionaldehyde[31], of which $HO_2\cdots H_2O$ makes a well-studied example[19, 32-39]. An interesting result[40, 41] concerning this complex is that the HO_2 self-reaction can be up to three times faster in the presence of water, and since HO_2 radical may exist up to 30% in the form of $HO_2\cdots H_2O$.[20, 42, 43] Moreover, Vohringer-Martinez et al[44] is one of the first studies to demonstrate how a single water molecule can catalyze a radical-molecule reaction involving OH radical. Due to the similar chemical structure and property of oxygen and sulfur in the same family, HS radical survives the similar hydrogen bonding characteristics of the $HO\cdots H_2O$ complex. These situations stimulated our interest in modeling the gas-phase reaction of $H_2O\cdots HO_2\cdots HS$ ternary system, in which the single water molecule serves as a catalyst. Besides, some studies have shown that water dimers[45-47] and trimers[47] can also play a significant catalytic effect in hydrogen abstraction reactions and hydrolysis of sulfur dioxide due to their concentration are up to 9×10^{14} [48]and 2.6×10^{12} molecules cm^{-3} [49] at 292 K. Thus the investigation of the effect of water dimer and water trimer on the channel of $H_2S + {}^3O_2$ formations from the HO_2 + HS reaction will be the logical path to pursue.

In the present study, a detailed effect of water, water dimer and water trimer on the channel of $H_2S + {}^3O_2$ formations from the HO_2 + HS reaction is carried out at the CCSD(T)/6-311++G(3df,2pd)//B3LYP/6-311+G(2df,2p) level of theory. Based on the channel of the $H_2S + {}^3O_2$ formations without water vapor, water-assisted $H_2S + {}^3O_2$ formations become quite complex yielding four different reaction channels of $H_2O\cdots HO_2$ + HS, $HO_2\cdots H_2O$ + HS, $HS\cdots H_2O + HO_2$ and $H_2O\cdots HS + HO_2$. These water-assisted channels are evaluated by investigating direct hydrogen abstraction process and double hydrogen transfer mechanism, as well as the water-catalyzed processes with non-catalytic processes are compared to see whether the catalytic processes are also possible to occur in gas phase. In the presence of water dimer, the reactions of SH radical with $HO_2\cdots(H_2O)_2$, $HO_2\cdots(H_2O)_2$a complexes, or HO_2 radical with $HS\cdots(H_2O)_2$, and $HS\cdots(H_2O)_2$a complexes are found, and these processes are compared with the corresponding water-assisted and non-catalytic processes. Then in the presence of water trimer, only the reactions of SH radical with $HO_2\cdots(H_2O)_3$, $HO_2\cdots(H_2O)_3$a complexes are identified due to that the concentration of $HO_2\cdots(H_2O)_3$, $HO_2\cdots(H_2O)_3$a are much larger than those of $HS\cdots(H_2O)_3$, $HS\cdots(H_2O)_3$a, and the

results that the reactions of HS radical with $HO_2\cdots(H_2O)_2$, $HO_2\cdots(H_2O)_2$a complexes, are more favorable than the reactions of HO_2 radical with $HS\cdots(H_2O)_2$, and $HS\cdots(H_2O)_2$a complexes. Also, these water trimer-assisted processes are compared with those channels without and with catalyst *X* (*X* = H_2O and $(H_2O)_2$). Finally, the theoretical rate constants of the most favorable primary channel without and with catalyst *X* (*X* = H_2O, $(H_2O)_2$) and $(H_2O)_3$) are calculated to investigate the atmospheric relevance of water molecule's effect. Overall, this work may lead to a better understanding of the effects of water vapor and water clusters on gas-phase reactions under tropospheric conditions.

2. Computational methods

The electronic structure calculations were performed using Gaussian09[50] software. The geometries of all the reactants, the prereactive complexes, postreactive complexes, transition states and products are optimized at the B3LYP/6-311+G(2df,2p) level of theory, as well as the corresponding frequencies of the optimized geometries are computed at the same level to prove the characters of the transition states with one imaginary frequency and the stationary points without imaginary frequency. Moreover, the minimum energy path (MEP) is obtained at the B3LYP/6-311+G(2df,2p) level by the intrinsic reaction coordinate (IRC)[51-53] theory with a gradient step size of 0.01-0.05 $(amu)^{1/2}$bohr to confirm that the TS really connects to minima along the reaction path. In order to obtain the relative energies reliably, single point energies were performed using the CCSD(T)[54]/6-311++G (3df, 2pd) method at the B3LYP-optimized geometries.

To estimate the effect of water, water dimer and water trimer added, the rate constants of HO_2 + HS reaction without and with catalyst *X* (*X* = H_2O, $H_2O)_2$ and $(H_2O)_3$) were calculated using conventional transition state theory (TST)[55-57] with the Wigner tunneling correction. All of the TST rate constant calculations are performed using the VKLab program[58] coupled with the steady state approximation. As described in Eq. (9), the title reaction without and with catalyst *X* (*X* = H_2O, $(H_2O)_2$) and $(H_2O)_3$) all began with the formation of a pre-reactive complex before progressing through the transition state.

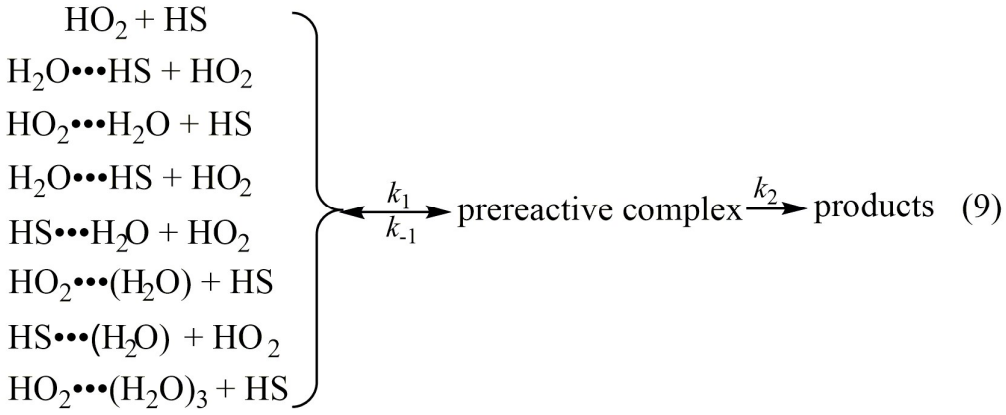

Assuming that the pre-reactive complexes in the title reaction without and with catalyst X (X = H_2O, $(H_2O)_2$) and $(H_2O)_3$) were in equilibrium with the corresponding reactants and were at steady state[59], the overall rate constants of the corresponding reaction processes were expressed as

$$k = \frac{k_1}{k_{-1} + k_2} k_2 \tag{10}$$

If $k_2 \ll k_{-1}$, the rate constant was rewritten as

$$k = \frac{k_1}{k_{-1} + k_2} k_2 = K_{eq} k_2 \tag{11}$$

where K_{eq} and k_2 was given by equation (12) and the VKLab program[58] , respectively.

$$K_{eq}(T) = s \frac{Q_{CR}}{Q_{R1} Q_{R2}} \exp\left(\frac{E_R - E_{CR}}{RT}\right) \tag{12}$$

In equation (12), the various Q values denote the partition functions of the pre-reactive complex, reactant R1 and R2, respectively. All partition functions are obtained using B3LYP/6-311+G(2df,2p) method. E_R, E_{CR} stand for the total energies of the reactants and complexes, respectively; σ is the symmetry factor. Computational details of the rate constant were shown in the supporting information.

3. Results and discussion

The transition states in each reaction channel were denoted by "TS" followed by a number, and intermediates were denoted by "IM" followed by a number. The letter "a" was used to distinguish the transition states and pre-reactive intermediates that were conformers of each other and therefore had the same features; a species in the presence of a water molecule, water dimmer and water trimer was respectively

denoted by a "W", "WW", and "WWW" postfix.

3.1 Potential energy surfaces for the channel of $H_2S + {}^3O_2$ formations from the $HO_2 + HS$ reaction

The reaction between HO_2 and HS was investigated theoretically in our previous report,[17] and the channel of the $H_2S + {}^3O_2$ formations on the triplet potential energy surface was identified as the most favorable channel. In this study, we reinvestigated the channel of the $H_2S + {}^3O_2$ formations at the same level to determine the outcome of the major channel of the HO_2 + HS reaction when a single water molecule, water dimer, and water trimer was respectively present. As seen in Fig. 1, regarding Channel R1, two elementary reaction paths were identified for the channel of the $H_2S + {}^3O_2$ formations, depending on how the HS radical approached HO_2. As seen in Fig. 1, a weak hydrogen bond between the H atom of HO_2 and the S atom of HS (with a computed S···H bond distance of 2.30 Å at the B3LYP/6-311+G(2df,2p) level) was respectively present in ^{3}IM1 and ^{3}IM1a, and their relative energies to the reactants (HO_2 and HS) were -3.0 kcal·mol^{-1}. Starting from ^{3}IM1 and ^{3}IM1a, the H atom of HO_2 attacked the S atom of HS through transition state ^{3}TS1 and ^{3}TS1a to form the $H_2S + {}^3O_2$ formations. From an energetic standpoint, Fig. 1 shows that at 0 K, the two transition states ^{3}TS1 and ^{3}TS1a were predicted to be 1.2 kcal·mol^{-1} below the energies of the reactants. The present study below mainly focuses on the catalytic roles of water, water dimer and water trimer in the channel of the $H_2S + {}^3O_2$ formations from the HO_2 + HS reaction in tropospheric conditions.

3.2 Geometrical analysis for the reactants of monomers, binary complexes, trinary complexes and quadruple complexes

For the HO_2 + HS reaction without and with catalyst X (X = H_2O, $(H_2O)_2$ and $(H_2O)_3$), Fig. 2 shows the optimized geometrical reactants of the monomers (H_2O, HO_2 and HS), binary complexes ($H_2O\cdots HO_2$, $HO_2\cdots H_2O$, $HS\cdots H_2O$, $HS\cdots H_2O$, and $H_2O\cdots H_2O$), trinary complexes ($HO_2\cdots(H_2O)_2$, $HS\cdots(H_2O)_2$ and $(H_2O)_3$), and quadruple complexes ($HO_2\cdots(H_2O)_3$ and $HS\cdots(H_2O)_3$) which are in good agreement with available experimental results[48, 60]. The discrepancies between the calculations and the experimental values are less than 0.06 Å (bond length) and 1.2° (bond angle).

For the binary complex of $H_2O\cdots HO_2$, a global minimum geometry of a five-membered ring-like structure via the formation of two hydrogen bonds (H1···O3 and H3···O1) was obtained, which is consistent with the geometry reported

previously[20, 61-63]. The bonding energy of $H_2O\cdots HO_2$ was 6.9 kcal·mol^{-1}, which agrees well with previous values[20, 61]. For binary complex reactants of $HO_2\cdots H_2O$, $HS\cdots H_2O$ and $H_2O\cdots HS$, their bonding energy was respectively 1.9, 1.7, and 1.6 kcal·mol^{-1}, which were less stable than the $H_2O\cdots HO_2$ complex with a single hydrogen bond involved.

Water dimer has one hydrogen bond (H2⋯O6, 1.96 Å), and its bonding energy is 3.1 kcal·mol^{-1}, which agree very well with previous values[48, 64-68]. This complex is considered as one of the initial reactants in water dimer–assisted HO_2 + HS reaction system because of its large concentration (about 7.18×10^{13} molecules·cm^{-3} as listed in Table 1). For the complexes $HO_2\cdots(H_2O)_2$ and $HS\cdots(H_2O)_2$, four stable geometries (denoted as $HO_2\cdots(H_2O)_2$, $HO_2\cdots(H_2O)_2$a, $HS\cdots(H_2O)_2$, and $HS\cdots(H_2O)_2$a respectively) were obtained by adding HO_2 or HS to the water dimer ($H_2O\cdots H_2O$). In these three-body complexes, both HO_2 (HS) radical and water dimer act as a single donor and a single acceptor of hydrogen bond to form a quasi-planar network. It was noteworthy that the geometrical structures both of the complexes $HO_2\cdots(H_2O)_2$ ($HO_2\cdots(H_2O)_2$, $HO_2\cdots(H_2O)_2$a) and complexes $HS\cdots(H_2O)_2$ ($HS\cdots(H_2O)_2$, and $HS\cdots(H_2O)_2$a) were mainly differing in the relative orientations of the two dangling hydrogen atoms of water dimer with the bonding energies of 12.6 ($HO_2\cdots(H_2O)_2$, and $HO_2\cdots(H_2O)_2$a) and 4.3 ($HS\cdots(H_2O)_2$ and $HS\cdots(H_2O)_2$a) kcal·mol^{-1}.

Water trimer has three hydrogen bonds with the bonding energy of 7.7 kcal·mol^{-1}. Its geometrical parameters and bonding energy compare quite well with the recently reported values from the literature[48, 65, 67]. For the complexes $HO_2\cdots(H_2O)_3$ and $HS\cdots(H_2O)_3$, four stable geometries (denoted as $HO_2\cdots(H_2O)_3$, $HO_2\cdots(H_2O)_3$a, $HS\cdots(H_2O)_3$, and $HS\cdots(H_2O)_3$a respectively) were obtained by adding HO_2 or HS to the water trimer $(H_2O)_3$. In these four-body complexes, similar with $HO_2\cdots(H_2O)_2$, $HO_2\cdots(H_2O)_2$a, $HS\cdots(H_2O)_2$, and $HS\cdots(H_2O)_2$a, both HO_2 (HS) radical and water trimer act as a single donor and a single acceptor of hydrogen bond to form a quasi-planar network with the bonding energies of 12.5 ($HO_2\cdots(H_2O)_3$, $HO_2\cdots(H_2O)_2$a), 3.8 ($HS\cdots(H_2O)_2$, $HS\cdots(H_2O)_2$a) kcal·mol^{-1}.

3.3 Mechanism for water-assisted the channel of $H_2S + {}^3O_2$ formations

In the presence of one water vapor, both HO_2 and HS radicals can interact with it via hydrogen bonds to form corresponding two-body complexes in the entrance channels. As shown in Fig. 2 and Table 1, four two-body complexes, viz. $HO_2\cdots H_2O$,

$H_2O\cdots HO_2$, $HS\cdots H_2O$ and $H_2O\cdots HS$, have been found. These two-body complexes can further react with the third species to form corresponding three-body complexes. Thus, when one water vapor was introduced into the channel of $H_2S + {}^3O_2$ formations from the HO_2+ HS reaction, four possible types of bimolecular reactions were considered as follows:

$$H_2O\cdots HO_2 + HS \rightarrow H_2O + H_2S + {}^3O_2 \quad (13)$$

$$HO_2\cdots H_2O + HS \rightarrow H_2O\cdots H_2S + {}^3O_2 \quad (14)$$

$$HS\cdots H_2O + HO_2 \rightarrow H_2S\cdots H_2O + {}^3O_2 \quad (15)$$

$$H_2O\cdots HS + HO_2 \rightarrow H_2O\cdots H_2S + {}^3O_2 \quad (16)$$

The four bimolecular reactions give rise to four major reaction channels (labeled as Channels RW1, RW2, RW3 and RW4) shown in Figs. 3, and 4. Thus four water-assisted channels were to describe the effect of water molecule on the channel of the $H_2S + {}^3O_2$ formations from the HO_2 + HS reaction under atmospheric conditions.

3.3.1 Water-assisted the channel of $H_2S + {}^3O_2$ formations occurring through the $H_2O\cdots HO_2$ + HS and $HO_2\cdots H_2O$ + HS reaction

The potential energy profile for water-assisted the channel of $H_2S + {}^3O_2$ formations occurring through $H_2O\cdots HO_2$ + HS (Channel RW1) and $HO_2\cdots H_2O$ + HS (Channel RW2) reactions can be seen in Fig. 3. For Channel RW1, by collision of $H_2O\cdots HO_2$ with HS, two kinds of reaction types have been found, which were labeled as Channel RW1a and Channel RW1b. Regarding to Channel RW1a, starting from $H_2O\cdots HO_2$ + HS reactants, hydrogen-bonded complexes ^{3}IMW1 and ^{3}IMW1a are formed by the interaction between the H atom of the HS radical and the terminal O atom of the HO_2 moiety in the $HO_2\cdots H_2O$ complex, with a bonding energy of 2.6 kcal·mol^{-1}. After a flat potential energy surface through ^{3}TSW1 and ^{3}TSW1a, with a small energy barrier of 0.3-0.4 kcal·mol^{-1}, the formation of complexes ^{3}IMW2 and ^{3}IMW2a are formed via three hydrogen bonds, in which the H_2O, HS and HO_2 moieties serve as the hydrogen bond donor and hydrogen bond acceptor simultaneously. Both ^{3}IMW2 and ^{3}IMW2 have seven member cyclic structures with a binding energy of 3.3 and 3.4 kcal·mol^{-1} relative to $H_2O\cdots HO_2$ + HS reactants, respectively, as shown in Fig. 3(a). After complexes of ^{3}IMW2 and ^{3}IMW2a, Channel RW1a goes on through transition states ^{3}TSW2 and ^{3}TSW2a in which the water acts as a bridge for the hydrogen transfer from the HO_2 to the SH radical, and as the water molecule accepts the hydrogen from HO_2, it simultaneously donates another hydrogen atom to the SH radical. The energy

of transition states ^{3}TSW2 and ^{3}TSW2a is respectively 6.3 and 6.2 kcal·mol^{-1} above the $H_2O\cdots HO_2$ + HS reactants.

Fig. 3(b) illustrates the PES profile of water-assisted Channel RW1b, including the corresponding geometries of stationary points. Regarding to Channel RW1b, the reaction of $H_2O\cdots HO_2$ + HS entry channel proceeds through the formation of the pre-reactive complexes ^{3}IMW3 and ^{3}IMW3a and the transition states ^{3}TSW3 ^{3}TSW3a before the formation of complexes ^{3}IMW4 and ^{3}IMW4a, and the subsequent unimolecular conversion to $H_2O\cdots H_2S$ and $^3O_2$, which is similar to the nitric acid-catalyzed hydrolysis[69, 70]of SO_3 and HCHO. The complexes ^{3}IMW3 and ^{3}IMW3a are computed to be 2.7 kcal·mol^{-1} below the reactants $H_2O\cdots HO_2$ + HS in Table S4 and Fig. 3(b). Similar with the rearrangement from ^{3}IMW1 to ^{3}IMW2 in Channel RW1a, the complex ^{3}IMW3 (^{3}IMW3a) which is stabilized via two hydrogen bonds and one van der Waals interaction is rearranged into its isomer ^{3}IMW4 (^{3}IMW4a) through ^{3}TSW3 (^{3}TSW3a) with a the barrier of about 0.2 (0.3) kcal·mol^{-1} relative to the complex ^{3}IMW3 (^{3}IMW3a).

^{3}IMW4 and ^{3}IMW4a complexes have similar seven member cyclic structures as ^{3}IMW2 and ^{3}IMW2a except that the SH radical and the water molecule have exchanged positions. In ^{3}IMW4 and ^{3}IMW4a complexes, hydrogen from the HS radical is hydrogen-bonded to the oxygen atom in the water molecule, and the hydrogen of the HO_2 radical forms a weak interaction with the S atom of HS radical to complete the cyclic structure, as shown in Fig. 3(b) and Fig. S3. The relative energies of complex ^{3}IMW4 and ^{3}IMW4a to HS + $HO_2\cdots H_2O$ reactants are -3.0 kcal·mol^{-1}. Following the complexes ^{3}IMW4 and ^{3}IMW4a, Channel RW1b proceeds through transition states ^{3}TSW4 and ^{3}TSW4a to produce the product of $H_2O\cdots H_2S$ + $^3O_2$ after respectively climbing the barrier height of 6.1 and 5.9 kcal·mol^{-1}. In the transition states ^{3}TSW4 and ^{3}TSW4a, the seven-membered ring structure is still conserved. Interesting, differently from transition states ^{3}TSW2 and ^{3}TSW2a in Channel RW1a that the S of HS indirectly abstracts the H atom of HO_2, and the water acts as a bridge for the hydrogen transfer from the HO_2 to the HS radical, transition states ^{3}TSW4 and ^{3}TSW4a in Channel RW1b contain a direct hydrogen abstraction by the S atom of HS radical abstracted the H atom of HO_2 moiety in $H_2O\cdots HO_2$ two-body complex. Such mechanism discrepancy between Channels RW1a and RW1b may lead that the energy of transition states ^{3}TSW2 and ^{3}TSW2a is

respectively 3.2 and 3.3 kcal·mol^{-1} higher than that of ^{3}TSW4 and ^{3}TSW4a. This situation can be seen in our previous reports[21, 61, 62, 71].

The second channel (Channel RW2, Fig. 3(c)) began with the formation of complexes ^{3}IMW5 and ^{3}IMW5a via the $HO_2\cdots H_2O$ complex reacting with HS. The bonding energy of complexes ^{3}IMW5 and ^{3}IMW5a relative to the $HO_2\cdots H_2O$ + HS reactants is 4.1 and 4.2 kcal·mol^{-1}, respectively, as shown in Fig. 3(c) and Table S4. In view of geometry, complexes ^{3}IMW5 and ^{3}IMW5a were stabilized by an additional weak hydrogen bond (2.26 Å) between the H atom of HO_2 moiety in $HO_2\cdots H_2O$ bimolecular complex and the S atom of HS radical. Similar to the geometrical differences between ^{3}IM1 and ^{3}IM1a (Fig. 1), the main discrepancy of the two three-body complexes (^{3}IMW5 and ^{3}IMW5a) in Fig. S3 remains locate in the relative orientation of the H atom of HS radical. Complexes ^{3}IMW5 and ^{3}IMW5a then respectively react via transition states ^{3}TSW5 and ^{3}TSW5a, which are similar in structure to the naked transition states ^{3}TS1 and ^{3}TS1a where the hydrogen is directly abstracted by the HS radical. Compared with the naked transition states ^{3}TS1 and ^{3}TS1a, the additional water molecule in transition states ^{3}TSW5 and ^{3}TSW5a is hydrogen bonded to the oxygen atom of HO_2 radical. Such a weak hydrogen bond (O1⋯H2, 2.14 Å) interaction may lead to the fact that the energy of these transition states to $HO_2\cdots H_2O$ + HS reactants is higher by 1.1-1.2 kcal·mol^{-1} than that of ^{3}TS1 (^{3}TS1a) to the HO_2 + HS reactants. However, the $HO_2\cdots H_2O$ + HS (Channel RW2) reaction can occur easily with small relative energy of ^{3}TSW5 (0.0 kcal·mol^{-1}) and ^{3}TSW5a (-0.1 kcal·mol^{-1}) to $HO_2\cdots H_2O$ + HO_2 reactants. The similar reaction channel of $HO_2\cdots H_2O$ + HO_2 has been reported in our previous work[62], where the additional reactions of $HO_2\cdots H_2O$ + HO_2 were also not neglected, with barrier heights between 1.10 and 1.79 kcal·mol^{-1}, and the estimated reaction rate constants 1–2 orders of magnitude larger than the naked reaction estimates. Thus the atmospheric relevance of $HO_2\cdots H_2O$ + HS reaction (Channel RW2) needs to further kinetic studies. Following transition states ^{3}TSW5 and ^{3}TSW5a, post reactive complexes ^{3}IMFW5 and ^{3}IMFW5a are formed with the bonding energies of 40.3 and 40.6 kcal·mol^{-1}. Fig. 3(c) and Fig. S3 shows that ^{3}IMFW5 has two hydrogen bonds, the first between one H atom of H_2O and one O atom of $^3O_2$; the second one between one H atom of H_2S and one O atoms of $^3O_2$. Complex ^{3}IMFW5 (^{3}IMFW5a) dissociates quickly to produce H_2O + H_2S·+ $^3O_2$, which lie 39.8 kcal·mol^{-1} below the energy of $HO_2\cdots H_2O$ + HS reactants.

3.3.2 Water-assisted the channel of $H_2S + {}^3O_2$ formations occurring through $HS\cdots H_2O + HO_2$ and $H_2O\cdots HS + HO_2$ reactions

Beyond water-assisted reaction channels described above, two additional water-assisted channels of $H_2S + {}^3O_2$ formation were found by taking into account the bimolecular reactions of $HS\cdots H_2O + HO_2$ (Channel RW3) and $H_2O\cdots HS + HO_2$ (Channel RW4). As far as Channel RW3 (Fig. 4(a)), starting from $HS\cdots H_2O + HO_2$ reactants, the sulfur atom of HS moiety in $HS\cdots H_2O$ complex directly extracts the H atom of HO_2 radical, occurring through the two different transition state ^{3}TSW6 and ^{3}TSW6a. From an energetic point of view, transition states ^{3}TSW6 and ^{3}TSW6a laid 5.1 and 5.5 kcal·mol^{-1} respectively above the $HS\cdots H_2O + HO_2$ reactants with the main geometrical difference in the relative orientation of the hydrogen atom of HS radical (the dihedral angles of ∠O(1)-O(2)-S-H(4) is -4.4°and -174.6° for ^{3}TSW6 and ^{3}TSW6a, respectively in Fig. S3). In view of the hydrogen abstraction, all these two elementary processes involved a direct hydrogen abstraction mechanism similar to the reaction without water. However, for transition states ^{3}TSW6 and ^{3}TSW6a, the hydrogen bond exists between the S atom of HS radical and one hydrogen atom of water molecule leads to that the spin density of S atom in these two transition state is much smaller than that in other water-assisted transition states, and is also smaller than that in ^{3}TS1 and ^{3}TS1a without water molecule. In other words, water vapor in transition states ^{3}TSW6 and ^{3}TSW6a is located away from the reaction center and cannot directly participate in the reaction. In such reactions, water acts as a spectator. This situation makes the hydrogen abstraction of Channel RW3 is much more difficult than other water-assisted channels and the naked reaction.

Regarding to the reaction of HO_2 with the $H_2O\cdots HS$ complex (Channel RW4), Fig. 4(b) shows that, hydrogen bond complex ^{3}IMW7 is formed with a computed binding energy of 8.2 kcal·mol^{-1} with respect to the $H_2O\cdots HS + HO_2$ reactants. Following complex ^{3}IMW7, Channel RW4 proceeds through transition state ^{3}TSW7 to produce the formations of $H_2O\cdots H_2S + {}^3O_2$ with the barrier height of 6.4 kcal·mol^{-1}. Differently from seven-membered ring transition state ^{3}TSW4, in transition state ^{3}TSW7, seven member cyclic structures is broken as the O1⋯H2 bond is elongated to 4.707 Å when the S atom of $H_2O\cdots HS$ abstracts the hydrogen of HO_2. Such geometrical discrepancy leads to that the energy of ^{3}TSW7 to $HO_2 + H_2O\cdots HS$ reactants is -1.8 kcal·mol^{-1}, which is lower by 4.9 kcal·mol^{-1} than that of ^{3}TSW4 to $HS + H_2O\cdots HO_2$ reactants. However, due to the lower concentration of $H_2O\cdots HS$

complex (71.5 molecules·cm^{-3} in Table 1), the catalytic effect of water in Channel RW4 need to further kinetic studies.

As a result of the above findings of H_2S + $^3O_2$ formations with a water molecule, the channels occurring through the $HO_2\cdots H_2O$ + HS reactants may be of great atmospheric relevance due to its lower barrier and the larger concentrations of $HO_2\cdots H_2O$, whereas the channel occurring through $HS\cdots H_2O$ + HO_2 reactants may be negligible due to its larger barrier. Besides, though the concentration of $H_2O\cdots HO_2$ and $H_2O\cdots$HS complexes is much lower than that of $HO_2\cdots H_2O$, the atmospheric relevance of $H_2O\cdots HO_2$ + HS and $H_2O\cdots$HS + HO_2 reactions need to further kinetic studies due to their lower activation energy.

3.4 Mechanism for water dimer-catalyzed the channel of H_2S + $^3O_2$ formations

In the presence of water dimer, both HO_2 and HS radicals can interact with it via hydrogen bonds to form corresponding three-body complexes of $HO_2\cdots(H_2O)_2$, $HO_2\cdots(H_2O)_2$a, $HS\cdots(H_2O)_2$, and $HS\cdots(H_2O)_2$a in the entrance channels. As shown in Fig. 5 and Fig. S4, with the insertion of SH radical into $HO_2\cdots(H_2O)_2$, $HO_2\cdots(H_2O)_2$a complexes, or HO_2 radical into the $HS\cdots(H_2O)_2$, and $HS\cdots(H_2O)_2$a complexes, three water dimer-assisted channels have been found, which were labeled as Channels RWW1, RWW2, and RWW3. Similar to the instance of one water-assisted reaction, as listed in Table 1, the concentrations of $HO_2\cdots(H_2O)_2$, and $HO_2\cdots(H_2O)_2$a (1.90×10^4 molecules cm^{-3}) are much larger than those of $HS\cdots(H_2O)_2$ (2.90×10^{-3} molecules cm^{-3}) and $HS\cdots(H_2O)_2$a (5.47×10^{-3} molecules cm^{-3}) at 298 K. Thus herein we mainly discussed water dimer-assisted channels (Channels RWW1 and RWW2) occurring through $HO_2\cdots(H_2O)_2$ ($HO_2\cdots(H_2O)_2$a) + HS reactants, while water dimer-assisted channel RWW3 will be neglected due to the lower contraction of $HS\cdots(H_2O)_2$, and $HS\cdots(H_2O)_2$a complexes, and the highest barrier of Channel RWW3 among the three Channels RWW1, RWW2 and RWW3.

As for Channel RWW1, with the collision of SH radical with $HO_2\cdots(H_2O)_2$, $HO_2\cdots(H_2O)_2$a complexes, the reaction begins with formation of the hydrogen bonded complexes ^{3}IMWW1 and ^{3}IMWW1a, whose stability are computed to be 2.8 kcal·mol^{-1}. Then the reaction goes through transition state ^{3}TSWW1 and ^{3}TSWW1a with an energy barrier of 0.3 kcal·mol^{-1} respectively relative to ^{3}IMWW1 and ^{3}IMWW1a. After ^{3}TSWW1 and ^{3}TSWW1a, two nine-member ring pre-reactive complexes ^{3}IMWW2 and ^{3}IMWW2a will be formed. Compared with ^{3}IMW2 and

^{3}IMW2a complexes with one water molecule, ^{3}IMWW2 and ^{3}IMWW2a has similar structure with the substitution of one water by water dimer, and the relative energies of them are -2.7 kcal·mol^{-1} to $HO_2\cdots (H_2O)_2$ ($HO_2\cdots (H_2O)_2$a) + HS reactants, which is respectively larger by 0.6 and 0.7 kcal·mol^{-1} than that of ^{3}IMW2 and ^{3}IMW2a to $HO_2\cdots H_2O$ + HS reactants. Starting from ^{3}IMWW2 and ^{3}IMWW2a, with the H atom of HO_2 migrating to the adjacent SH group and the hydrogen bond breaking between the H atom of HS and the terminal O atom of HO_2, the reaction can proceed via transition states ^{3}TSWW2 and ^{3}TSWW2a to form the products of $H_2S\cdots(H_2O)_2$ + $^3O_2$ and $H_2S\cdots(H_2O)_2$a + $^3O_2$, respectively. ^{3}TSWW2 and ^{3}TSWW2a show six-membered ring structures with water dimer, S atom of HS and the H atom of HO_2 involved. The relative energies of ^{3}TSWW2 and ^{3}TSWW2a to $HO_2\cdots(H_2O)_2$ ($HO_2\cdots(H_2O)_2$a) + HS is 8.9 and 8.3 kcal·mol^{-1}, respectively, which is higher by 2.6 and 2.1 kcal·mol^{-1} than that of the water-assisted transition states ^{3}TSW2 and ^{3}TSW2a to $HO_2\cdots H_2O$ + HS reactants.

Similar to Channel RWW1, Channel RWW2 also proceeds through a stepwise mechanism to form $H_2S\cdots(H_2O)_2$ ($H_2S\cdots(H_2O)_2$a) + $^3O_2$. In the first step, the reaction begins with the formations of the hydrogen bonded complexes ^{3}IMWW3 and ^{3}IMWW3a by combining HS and $HO_2\cdots(H_2O)_2$ ($HO_2\cdots(H_2O)_2$a) complexes. The stabilization energies of ^{3}IMWW3 and ^{3}IMWW3a were 1.5 kcal·mol^{-1}. From the geometric point of view described in Fig. 5(b), similar to the complexes ^{3}IMWW1 and ^{3}IMWW1a, complexes ^{3}IMWW3 and ^{3}IMWW3a were also stabilized by one hydrogen bond between HS and $HO_2\cdots(H_2O)_2$ ($HO_2\cdots(H_2O)_2$a). However, the form of hydrogen bond in complexes ^{3}IMWW3 and ^{3}IMWW3a were different than that in ^{3}IMWW1 and ^{3}IMWW1a. For instance, the one-hydrogen-bond interaction in ^{3}IMWW3 occurred between O3 atom of $(H_2O)_2$ moiety in $HO_2\cdots(H_2O)_2$ complex and the H atom of HS radical. In contrast, the hydrogen bond involved in ^{3}IMWW1 was formed between the terminal O1 atom of HO_2 moiety in $HO_2\cdots(H_2O)_2$ complex and the H atoms of HS. These differences in hydrogen-bonding patterns may have arisen because the binding energies of ^{3}IMWW3 and ^{3}IMWW3a (Fig.5 and Table S7) reduce by 1.3 kcal·mol^{-1} than those of ^{3}IMWW1 and ^{3}IMWW1a. After formations of the prereactive complexes ^{3}IMWW3 and ^{3}IMWW3a, Channel RWW2 progresses through the elementary reactions ^{3}TSWW3 and ^{3}TSWW3a to from two nine-membered ring pre-reactive complexes ^{3}IMWW4 and ^{3}IMWW4a. From geometrical point of view,

complexes ^{3}IMWW4 and ^{3}IMWW4a have similar quasi-planar structures as those of ^{3}IMW4 and ^{3}IMW4a (Fig. 4(b)), with the additional water molecule inserted between HO_2 and HS. The binding energy of ^{3}IMWW4 (^{3}IMWW4a) is 3.6 kcal·mol^{-1}, which is larger by 0.6 kcal·mol^{-1} that of ^{3}IMW4 (^{3}IMW4a). Besides, similar with the difference between complexes ^{3}IMW2 (^{3}IMW2a) and ^{3}IMW4 (^{3}IMW4a) with a water molecule, ^{3}IMWW4 and ^{3}IMWW4a has a similar nine member cyclic structure as ^{3}IMWW2 (^{3}IMWW2a) except that the SH radical and the water dimer have exchanged positions.

Transition states ^{3}TSWW4 (^{3}TSWW4a) were found between ^{3}IMWW4 (^{3}IMWW4a) and the products formation of $H_2S\cdots(H_2O)_2 + {}^3O_2$ ($H_2S\cdots(H_2O)_2a + {}^3O_2$). Differently from transition states ^{3}TSWW2 and ^{3}TSWW2a, at the transition states ^{3}TSWW4 and ^{3}TSWW4a, nine-member ring structures were not broken when the hydrogen abstraction occurs by the S atom of HS radical abstracted the H atom of HO_2 radical. Such geometrical discrepancy between ^{3}TSWW4 (^{3}TSWW4a) and ^{3}TSWW2 (^{3}TSWW2a) leads to that the relative energies of ^{3}TSWW4 and ^{3}TSWW4a is respectively lower by 2.9 and 2.1 kcal·mol^{-1} that those of ^{3}TSWW2 and ^{3}TSWW2a. This suggests that water dimer-assisted the channel of $H_2S + {}^3O_2$ formations mainly occurs through Channel RWW2.

As a result of the above findings of $H_2S + {}^3O_2$ formations with water dimer, the channels occurring through the $SH + HO_2\cdots(H_2O)_2$ ($HO_2\cdots(H_2O)_2a$) reactants may be of great atmospheric relevance, whereas channels occurring through $HO_2 + HS\cdots(H_2O)_2$ ($HS\cdots(H_2O)_2a$) reactants may be negligible due to the high barrier heights and their low concentration. Besides, water dimer-assisted the channel of $H_2S + {}^3O_2$ formations mainly occurs through Channel RWW2.

3.5 Mechanism for water trimer-catalyzed the channel of $H_2S + {}^3O_2$ formations

It is of interest to known whether water trimer will effect the $H_2S + {}^3O_2$ formations from the HO_2 + HS reaction. Thus, based on the discussed results above that the reactions of SH radical with $HO_2\cdots(H_2O)_2$, $HO_2\cdots(H_2O)_2a$ complexes are more favorable than the reactions of HO_2 radical with $HS\cdots(H_2O)_2$, and $HS\cdots(H_2O)_2a$ complexes in the presence of water dimer, only the reactions of SH radical with $HO_2\cdots(H_2O)_3$, $HO_2\cdots(H_2O)_3a$ complexes are investigated for the channel of $H_2S + {}^3O_2$ formations with water trimer due to that the concentration (Table 1) and the stabilized energy (Fig. 6) of $HO_2\cdots(H_2O)_3$, $HO_2\cdots(H_2O)_3a$ are much larger than those of $HS\cdots(H_2O)_3$, $HS\cdots(H_2O)_3a$. The schematic potential energy surfaces for water

trimer-assisted the channel of H_2S + $^3O_2$ formations were drawn in Fig. 6; Table S9 contains the zero point energy (ZPE), relative energies, enthalpies, and free energies at 298 K for the corresponding stationary points for H_2S + $^3O_2$ formations in the reactions of SH + $HO_2\cdots(H_2O)_3$ ($HO_2\cdots(H_2O)_3$a) reactions.

Regarding the major reaction of $HO_2\cdots(H_2O)_3$ ($HO_2\cdots(H_2O)_3$a) + HS, the pre-reactive complexes ^{3}IMWWW1 and ^{3}IMWWW1a were formed with the energy of about -3.0 kcal·mol^{-1} with respect to the $HO_2\cdots(H_2O)_3$ ($HO_2\cdots(H_2O)_3$a) + HS. Starting from complexes ^{3}IMWWW1 and ^{3}IMWWW1a, the reaction occurs via transition state ^{3}TSWWW1 (^{3}TSWWW1a) and to form a complex ^{3}IMWWW2 (^{3}IMWWW2a) from ^{3}IMWWW1 (^{3}IMWWW1a) with a barrier of 4.9 kcal·mol^{-1} relative to the pre-reactive complex ^{3}IMWWW1 (^{3}IMWWW1a). This step involves a geometric rearrangement that plays a crucial role in $HO_2\cdots(H_2O)_3$ ($HO_2\cdots(H_2O)_3$a) + HS reaction. ^{3}IMWWW2 (^{3}IMWWW2a) is less stabilized than ^{3}IMWWW1 (^{3}IMWWW1a) by 2.2-2.3 kcal·mol^{-1}. From a geometric point of view, complexes ^{3}IMWWW2 and ^{3}IMWWW2a have similar quasi-planar structures as those of ^{3}IMWW4 and ^{3}IMWW4a, with the additional water molecule inserted between HO_2 and HS. The relative energies of ^{3}IMWWW2 and ^{3}IMWWW2a are -0.8 and -0.7 kcal·mol^{-1} with respect to $HO_2\cdots(H_2O)_3$ ($HO_2\cdots H_2O)_3$a) + HS.

Transition state ^{3}TSWWW2 (^{3}TSWWW2a) was found between ^{3}IMWWW2 (^{3}IMWWW2a) and the products $H_2S\cdots(H_2O)_2$ ($H_2S\cdots(H_2O)_2$a) and $^3O_2$. At ^{3}TSWWW2 (^{3}TSWWW2a), a hydrogen abstraction reaction occurs by the S atom of HS abstracted the H atom HO_2 radical as that in ^{3}TSWW4 (^{3}TSWW4a) with the additional water molecule inserted between HO_2 and HS. ^{3}TSWWW2 (^{3}TSWWW2a) lies 7.3 (7.5) kcal·mol^{-1} above the $HO_2\cdots(H_2O)_3$ ($HO_2\cdots(H_2O)_3$a) + HS reactants, which is 1.3 kcal·mol^{-1} higher in energy than the relative energy of ^{3}TSWW4 (^{3}TSWW4a) to $HO_2\cdots(H_2O)_2$ ($HO_2\cdots(H_2O)_2$a) + HS reactants.

3.6 kinetics and Application in Atmospheric Chemistry

Beyond above mechanisms without and with catalyst *X* (*X* = H_2O, $(H_2O)_3$ and $(H_2O)_3$), another aim of our work was to study the influence of water, water dimer and water trimer on the HO_2 + HS reaction under atmospheric conditions. Thus, Table 2 and Table 3 respectively lists the calculated rate constants and effective rate constants for the title reaction with a single water vapor, meanwhile the rate constants and effective rate constants for the H_2S + $^3O_2$ formation with water dimer and water trimer

are shown in Table 4. Besides, detail information regarding every channel for the title reaction lists in the Supporting Information (Tables S2, S5, S9, S10, and S14).

Table 2 shows that, for the HO_2 + HS reaction in the presence of a water vapor, the rate constants of $H_2O\cdots HO_2$ + HS reaction (Channel RW1, k_{RW1}) and $HO_2\cdots H_2O$ + HS reaction (Channel RW2, k_{RW2}) were larger by 5-10 orders of magnitude than those of $HS\cdots H_2O$ + HO_2 (Channel RW3, k_{RW3}) and HO_2 + $H_2O\cdots HS$ reaction (Channel RW4, k_{RW4}) within the calculated temperature range. Besides, the rate constant of Channels RW1 and RW2 was larger than that of the naked reaction (Channel R1), given that the ratio of k_{RW1}/k_{R1}, and k_{RW2}/k_{R1} was $18.4 - 9.91\times10^2$, and 1.06×10^2-1.73×10^2, respectively. This indicated that, for Channels RW1, and RW2, the single water molecule has a positive influence on enhancing the rate of the H_2S + $^3O_2$ formations.

To obtain a more complete understanding of the influence of a water vapor on the title reaction, it is necessary to compare the title rate in the absence of a water vapor with the effective rates of the corresponding reactions in the presence of a water vapor. The rate for the title reaction without a water vapor was expressed as

$$v_{R1}=k_{R1}\,[HO_2][HS] \quad (17)$$

While the rate for water-assisted reactions via Channels RW1 and Channels RW2 were written as

$$v_{RW1}=k_{RW1}\,[H_2O\cdots HO_2][HS]=k'_{RW1}\,[HO_2][HS] \quad (18)$$

$$v_{RW2}=k_{RW2}\,[HO_2\cdots H_2O][HS]=k'_{RW2}\,[HO_2][HS] \quad (19)$$

In these equations, $k'_{RW1}=k_{RW1}\ K_{eq}(H_2O\cdots HO_2)[H_2O]$, and $k'_{RW2}=k_{RW2}\ K_{eq}(HO_2\cdots H_2O)[H_2O]$. $K_{eq}(H_2O\cdots HO_2)$ and $K_{eq}(HO_2\cdots H_2O)$ was respectively the equilibrium constants for the formation of the $H_2O\cdots HO_2$ and $HO_2\cdots H_2O$ complex; $[H_2O]$ was the concentration of water vapor[55]. As seen in Table 3, within the temperature range of 240.0–425.0 K, the total rate constant, k_{tot}, is plotted alongside k_R, k'_{RW1} and k'_{RW2}.

$$k_{tot} = k_R + k'_{RW1} + k'_{RW2} \quad (20)$$

Calculated results in Table 3 show that the branching ratio of k'_{RW1}/k_{total} increases gradually from 0.36% at 240 K to 3.00% at 425 K, while k'_{RW2}/k_{total} (0.01% at 240 K) increases to 35.0% at 425 K, respectively. The above results indicate that Channel RW1 ($H_2O\cdots HO_2$ + HS reaction) is the main water-assisted channel of H_2S + $^3O_2$ formations within the temperature range of 240-308 K, while Channel RW2

($HO_2\cdots H_2O$ + HS reaction) are main products within the temperature of 308-425 K. This situation is similar with our previous report [62] that both reactions of $H_2O\cdots HO_2$ + HO_2 and $HO_2\cdots H_2O$ + HO_2 were also not neglected in water assisted the process of $^3O_2$ formation from HO_2 + HO_2 reaction. Besides, the result in Table 3 is estimated that at low temperature, such as 240 K the enhancement factor of water vapor is only 0.37%. While at high temperature, such as 425 K, the positive water vapor effect enhances up to 38.00%, showing at high temperatures the positive water effect is obvious under atmospheric conditions.

In addition to study the effect of water dimer and water trimer on the H_2S + $^3O_2$ formations in HO_2 + HS reaction, Table 4 lists the rate constants and effective rate constants for the H_2S + $^3O_2$ formations with water dimer and water trimer. As seen in Table 4, the rate constant of $HO_2\cdots(H_2O)_2$ ($HO_2\cdots(H_2O)_2$a) + SH reaction occurring through Channel RWW2 are larger than that occurring through Channel RWW1 given that the ratio of k_{RWW2}/k_{RWW1} and k_{RWW2a}/k_{RWW1a} was 2.76×10^3-22.2 and 8.48×10^2-16.3, respectively. Besides, the rate constant of Channel RWW2 are also larger that the rate constant of $HS\cdots(H_2O)_2$ ($HS\cdots(H_2O)_2$a) +HO_2 reaction occurring through Channel RWW3, given that the ratio of k_{RWW2}/k_{RWW3} and k_{RWW2a}/k_{RWW3a} was 1.81×10^5-3.57×10^4 and 1.87×10^5-7.89×10^4, respectively. This indicates that the catalytic effect of water dimer was mainly taken from Channel RWW2 in $HO_2\cdots(H_2O)_2$ ($HO_2\cdots(H_2O)_2$a) +SH reaction. Compared with the rate constants (k_{RWWW1} and k_{RWWW1a}) of $HO_2\cdots(H_2O)_3$ ($HO_2\cdots(H_2O)_3$a) +SH reaction occurring through Channel RWWW1, the rate constants (k_{RWW2} and k_{RWW2a}) of Channel RWW2 with water dimer is respectively larger by 13.2-1.01 and 9.80-0.47 times.

In order to obtain a more complete understanding of the influence of water dimer and water trimer on the title reaction, the rate for water dimer-assisted reactions via Channels RWW2 and water trimer-assisted reactions via Channels RWWW1 is respectively written as

$$v_{RWW2}=k_{RWW2}\,[HO_2\cdots(H_2O)_2][HS] + k_{RWW2a}\,[HO_2\cdots(H_2O)_2a][HS]$$
$$=k'_{RWW2}\,[HO_2][HS] + k'_{RWW2a}\,[HO_2][HS] \quad (21)$$

$$v_{RWWW1}=k_{RWWW1}\,[HO_2\cdots(H_2O)_3][HS] + k_{RWWW1a}\,[HO_2\cdots(H_2O)_3a][HS]$$
$$=k'_{RWWW1}\,[HO_2][HS] + k'_{RWWW1a}\,[HO_2][HS] \quad (22)$$

In these equations, $k'_{RWW2} = k_{RWW2}\,K_{eq}(HO_2\cdots(H_2O)_2)[(H_2O)_2]$; $k'_{RWW2a} = k_{RWW2a}\,K_{eq}(HO_2\cdots(H_2O)_2a)[(H_2O)_2]$; $k'_{RWWW1} = k_{RWWW1}\,K_{eq}(HO_2\cdots(H_2O)_3)[(H_2O)_3]$ and $k'_{RWWW1a} = k_{RWWW1a}\,K_{eq}(HO_2\cdots(H_2O)_3a)[(H_2O)_3]$. $K_{eq}(HO_2\cdots(H_2O)_2)$,

$K_{eq}(HO_2\cdots(H_2O)_2a)$, $K_{eq}(HO_2\cdots(H_2O)_3)$ and $K_{eq}(HO_2\cdots(H_2O)_3a)$ was respectively the equilibrium constants for the formation of the $HO_2\cdots(H_2O)_2$, $HO_2\cdots(H_2O)_2a$, $HO_2\cdots(H_2O)_3$ and $HO_2\cdots(H_2O)_3a$ complexes. As seen in Table 4, within the temperature range of 240.0–425.0 K, the effective rate constant of Channel RWW2 ($k'_{RWW2} + k'_{RWW2a} = 8.76\times10^{-22}—5.92\times10^{-19}$ $cm^3\cdot molecule^{-1}\cdot s^{-1}$) was larger by 3-1 orders of magnitude than the value of $HO_2\cdots(H_2O)_3$ ($HO_2\cdots(H_2O)_3a$) +SH (Channel RWWW1, $k'_{RWWW1} + k'_{RWWW1a}$). Meanwhile, the sum value of k'_{RWW2} and k'_{RWW2a} was smaller by 7-12 orders of magnitude than the total effective rate constant of Channel RW1 (k'_{RW1}) and Channel RW2 (k'_{RW2}), indicating that the catalytic effect of single water is the largest among the effect of water, water dimer and water trimer, and the catalytic effect taken from water dimer and water trimer is neglected. However, the study of water dimer and water trimer in this article is important as it brings further molecular insight on how the reaction can take place at water clusters.

4. Summary and Conclusions

The channel of $H_2S + {}^3O_2$ formations from the HO_2 + HS reaction catalyzed by water, water dimer and water trimer are theoretically investigated using quantum chemical methods and the conventional transition state theory, which results in the following conclusions:

(a) For water-assisted reactions, the channels occurring through the $HO_2\cdots H_2O$ + HS reactants may be of great atmospheric relevance due to its lower barrier and the larger concentrations of $HO_2\cdots H_2O$, whereas the channel occurring through $HS\cdots H_2O$ + HO_2 reactants may be negligible due to its larger barrier. Besides, though the concentration of $H_2O\cdots HO_2$ and $H_2O\cdots HS$ complexes is much lower than that of $HO_2\cdots H_2O$, their atmospheric relevance of $H_2O\cdots HO_2$ + HS and $H_2O\cdots HS$ + HO_2 reactions need to further kinetic studies due to their lower activation energy.

(b) For water dimer-assisted reactions, the channels occurring through the SH + $HO_2\cdots(H_2O)_2$ ($HO_2\cdots(H_2O)_2a$) reactants may be of great atmospheric relevance, whereas channels occurring through HO_2 + $HS\cdots(H_2O)_2$ ($HS\cdots(H_2O)_2a$) reactants may be negligible due to the high barrier heights and their low concentration. Besides, water dimer-assisted the channel of $H_2S + {}^3O_2$ formations mainly occurs through Channel RWW2.

(c) The main reactions of SH radical with $HO_2\cdots(H_2O)_3$, $HO_2\cdots(H_2O)_3a$ complexes are investigated for $^3O_2 + H_2S$ formations with water trimer. For the rate

determining step, the apparent activation energy of SH + $HO_2\cdots(H_2O)_3$, $HO_2\cdots(H_2O)_3$a reaction is 7.3-7.5 kcal·mol^{-1}, which is higher by 1.3 kcal·mol^{-1} than that of $HO_2\cdots(H_2O)_2$ ($HO_2\cdots(H_2O)_2$a) + HS reactions.

(d) The catalytic effect of water, water dimer and water trimer is mainly taken from the effect of a single water vapor, due to the effective rate constant of water-assisted reaction was larger by 2-3, 5-6 orders of magnitude than the corresponding rate constant of water dimer-assisted reactions and water trimer-assisted reactions. Besides, the enhancement factor of water vapor is only 0.37% at 240 K, while at high temperature, such as 425 K, the positive water vapor effect enhances up to 38.04%.

Acknowledgments

This work was supported by the National Natural Science Foundation of China (No: 21207081, 21473108), the Funds of Research Programs of Shaanxi University of Technology (No: SLGQD13(2)-3, SLGQD13(2)-4) and Shandong Provincial Natural Science Foundation, China (No:ZR2012DQ001). Chen Yang and Xukai Feng contribute equally to this work.

References

[1] L. M. Stock, R. Wolny and B. Bal, *Energy & fuels*, 1989, **3**, 651-661.
[2] B. B. Majchrowicz, J. Yperman, J. Mullens and L. C. Van Poucke, *Anal Chem*, 1991, **63**, 760-763.
[3] J. Yan, J. Yang and Z. Liu, *Environ Sci Technol*, 2005, **39**, 5043-5051.
[4] I. I. Maes, G. Gryglewicz, H. Machnikowska, J. Yperman, D. V. Franco, J. Mullens and L. C. Van Poucke, *Fuel*, 1997, **76**, 391-396.
[5] A. Makishima and E. Nakamura, *Anal Chem*, 2001, **73**, 2547-2553.
[6] W. H. Calkins, *Fuel*, 1994, **73**, 475-484.
[7] C. Wilson and D. M. Hirst, *Prog. React. Kinet.*, 1996, **2**, 69-132.
[8] G. S. Tyndall and A. R. Ravishankara, *Atmos. Environ.*, 1991, **23**, 483-527.
[9] S. M. Resende and F. R. Ornellas, *J. Phys. Chem. A*, 2000, **104**, 11934-11939.
[10] S. M. Resende and F. R. Ornellas, *Chem Phys Lett*, 2000, **318**, 340-344.
[11] G. Black, *J. Chem. Phys.*, 1984, **80**, 1103-1107.
[12] R. Atkinson, D. L. Baulch, R. A. Cox, J. N. Crowley, R. F. Hampson, R. G. Hynes, M. E. Jenkin, M. J. Rossi and J. Troe, *Atmos. Chem. Phys.*, 2004, **4**, 1461-1738.
[13] S. C. Herndon, K. D. Froyd, E. R. Lovejoy and A. R. Ravishankara, *J. Phys. Chem. A*, 1999, **103**, 6778-6785.
[14] R. R. Friedl, W. H. Brune and J. G. Anderson, *J. Phys. Chem.*, 1985, **89**, 5505-5510.
[15] D. J. Nesbitt and S. R. Leone, *J. Chem. Phys.*, 1980, **72**, 1722-1732.
[16] L. G. S. Shum and S. W. Benson, *Int. J. Chem. Kinet.* , 1985, **17**, 749-761.
[17] Zhang Tianlei, Yang Chen, Feng Xukai, Wang Zhuqing, Wang Rui, Liu Qiuli, Zhang Peng and W. Wenliang, *Acta Phys Chim Sin*, 2016, **32**, 701-710.
[18] J. S. F. R. J. Buszek, J. M. Anglada, *Int Rev Phys Chem*, 2011, **30**, 335-369.
[19] A. M. English, J. C. Hansen, J. J. Szente and A. M. Maricq, *J. Phys. Chem. A*., 2008, **112**, 9220-9228.
[20] B. Long, X. F. Tan, Z. W. Long, Y. B. Wang, D. S. Ren and W. J. Zhang, *J. Phys. Chem. A.*, 2011, **115**, 6559-6567.
[21] T. L. Zhang, W. L. Wang, P. Zhang, J. Lu and Y. Zhang, *Phys. Chem. Chem. Phys.*, 2011, **13**, 20794-20805.
[22] V.-M. E, B. Hansmann, H. Hernandez, J. S. Francisco, J. Troe and B. Abel, *Science*, 2007, **315**, 497-501.
[23] R. J. Buszek, M. Torrent-Sucarrat, J. M. Anglada and J. S. Francisco, *J. Phys. Chem. A*, 2012, **116**, 5821-5829.
[24] J. Gonzalez, J. M. Anglada, R. J. Buszek and J. S. Francisco, *J. Am. Chem. Soc.*, 2011, **133**, 3345-3353.
[25] J. M. Anglada and J. Gonzalez, *Chem. Phys. Chem.*, 2009, **10**, 3034-3045.
[26] J. Gonzalez and J. M. Anglada, *J. Phys. Chem. A.*, 2010, **114**, 9151-9162.
[27] V.-M. E., B. Hansmann, H. Hernandez, J. S. Francisco, J. Troe and B. Abel, *Science*, 2007, **315**, 497-501.
[28] Sébastien Canneaux, Nathalie Sokolowski-Gomez, Eric Henon, F. Bohr and S. Dóbéb, *Phys. Chem. Chem.*

Phys. , 2004, **6**, 5172-5177.
[29] C. Iuga, J. R. Alvarez-Idaboy and A. Vivier-Bunge, *Chem. Phys. Lett.*, 2010, **501**, 11-15.
[30] S. Jørgensen and H. G. Kjaergaard, *J. Phys. Chem. A* 2010, **114**, 4857-4863.
[31] E. Vohringer-Martinez, E. Tellbach, M. Liessmann and B. Abel, *J. Phys. Chem. A.*, 2010, **114**, 9720-9724.
[32] Y. Tang, G. S. Tyndall and J. J. Orlando, *J. Phys. Chem. A*, 2009, **114**, 369-378.
[33] N. Butkovskaya, M.-T. Rayez, J.-C. Rayez, A. Kukui and G. L. Bras, *J. Phys. Chem. A*, 2009, **113**, 11327-11342.
[34] E. J. Hamilton, *J. Chem. Phys.*, 1975, **63**, 3682.
[35] S. Aloisio and J. S. Francisco, *J. Phys. Chem. A*, 1998, **102**, 1899-1902.
[36] S. Aloisio, J. S. Francisco and R. R. Friedl, *J. Phys. Chem. A*, 2000, **104**, 6597-6601.
[37] N. Kanno, K. Tonokura, A. Tezaki and M. Koshi, *J. Phys. Chem. A*, 2005, **109**, 3153-3158.
[38] K. Suma, Y. Sumiyoshi and Y. Endo, *Science*, 2006, **311**, 1278-1281.
[39] R. Zhu and M. C. Lin, *Chem phys lett*, 2002, **354**, 217-226.
[40] R. A. B. Cox, J. P., *J. Phys. Chem.*, 1979, **83**, 2560.
[41] C. C. Kircher and S. P. Sander, *J. Phys. Chem.*, 1984, **88**, 2082-2091.
[42] S. Aloisio and J. S. Francisco, *J. Phys. Chem. A*, 1998, **102**, 1899-1902.
[43] S. Aloisio, J. S. Francisco and R. R. Friedl, *J. Phys. Chem. A.*, 2000, **104**, 6597-6601.
[44] E. Vöhringer-Martinez, B. Hansmann, H. Hernandez, J. S. Francisco, J. Troe and B. Abel, *Science*, 2007, **315**, 497-501.
[45] B. Du and W. Zhang, *Comput. Theor. Chem.*, 2015, **1049**, 90-96.
[46] B. Du and W. Zhang, *Comput. Theor. Chem.*, 2015, **1069**, 77-85.
[47] L. P. Viegas and A. J. C. Varandas, *J. Phys. Chem. B* 2015, **DOI: 10.1021/acs.jpcb.5b07691**.
[48] M. E. Dunn, E. K. Pokon and G. C. Shields, *J. Am. Chem. Soc.*, 2004, **126**, 2647-2653.
[49] N. Goldman, R. S. Fellers, C. Leforestier and R. J. Saykally, *J. Phys. Chem. A*, 2001, **105**, 515-519.
[50] *M. J. Frisch, G. W. Trucks and J. A. Pople, et al., Gaussian 09, Revision A.01, Gaussian Inc., Pittsburgh, PA, 2009*.
[51] K. Fukui, *Acc. Chem. Res.*, 1981, **14**, 363-368.
[52] M. Page and J. W. McIver Jr, *J. Chem. Phys.*, 1988, **88**, 922-935.
[53] C. Gonzalez and H. B. Schlegel, *J. Chem. Phys*, 1989, **90**, 2154-2161.
[54] Y. S. Lee, S. A. Kucharski and R. J. Bartlett, *J. Chem. Phys.*, 1984, **81**, 5906-5912.
[55] B. C. Garrett and D. G. Truhlar, *J. Chem. Phys.*, 1979, **70**, 1593-1598.
[56] B. C. Garrett and D. G. Truhlar, *J. Am. Chem. Soc.*, 1979, **101**, 4534-4548.
[57] B. C. Garrett, D. G. Truhlar, R. S. Grev and A. W. Magnuson, *J. Phys. Chem.*, 1980, **84**, 1730-1748.
[58] *S. W. Zhang and N. T. Truong, VKLab version 1.0, University of Utah, Salt Lake City, 2001*.
[59] D. L. Singleton and R. J. Cvetanovic, *J. Am. Chem. Soc.*, 1976, **98**, 6812-6819.
[60] From the NIST ChemistryWebbook, http:// webbook.nist.gov/chemistry.
[61] T. Zhang, R. Wang, H. Chen, S. Min, Z. Wang, C. Zhao, Q. Xu, L. Jin, W. Wang and Z. Wang, *Phys. Chem. Chem. Phys.*, 2015, **17**, 15046-15055.
[62] T. Zhang, R. Wang, W. Wang, S. Min, Q. Xu, Z. Wang, C. Zhao and Z. Wang, *Comput. Theor. Chem.*, 2014, **1045**, 135-144.
[63] X. Chen, C. Tao, L. Zhong, Y. Gao, W. Yao and S. Li, *Chemical Physics Letters*, 2014, **608**, 272-276.
[64] A. Shank, Y. Wang, A. Kaledin, B. J. Braams and J. M. Bowman, *J. Chem. Phys.* , 2009, **130**, 144314.
[65] J. Gonzalez, M. Caballero, A. Aguilar-Mogas, M. Torrent-Sucarrat, R. Crehuet, A. Sole, X. Gimenez, S. Olivella, J. M. Bofill and J. M. Anglada, *Theor. Chem. Acc.*, 2011, **128**, 579-592.
[66] M. Torrent-Sucarrat, J. S. Francisco and J. M. Anglada, *J. Am. Chem. Soc.*, 2012, **134**, 20632-20644.
[67] R. M. Shields, B. Temelso, K. A. Archer, T. E. Morrell and G. C. Shields, *J. Phys. Chem. A*, 2010, **114**, 11725-11737.
[68] B. Ruscic, *J. Phys. Chem. A*, 2013, **117**, 11940-11953.
[69] F.-Y. Liu, X.-F. Tan, Z.-W. Long, B. Long and W.-J. Zhang, *RSC Adv.*, 2015, **5**, 32941-32949.
[70] B. Long, C.-R. Chang, Z.-W. Long, Y.-B. Wang, X.-F. Tan and W.-J. Zhang, *Chem. Phys. Lett.*, 2013, **581**, 26-29.
[71] T. L. Zhang, G. N. Li, W. L. Wang, Y. M. Du, C. Y. Li and J. Lu, *Computational and Theoretical Chemistry*, 2012, **991**, 13-21.

Table 1 Equilibrium Constants of Relevant $H_2O\cdots HO_2$, $HO_2\cdots H_2O$, $HS\cdots H_2O$, $H_2O\cdots HS$, $(H_2O)_2$, $HO_2\cdots(H_2O)_2$, $HO_2\cdots(H_2O)_2a$, $HS\cdots(H_2O)_2$, $HS\cdots(H_2O)_2a$, $(H_2O)_3$, $HO_2\cdots(H_2O)_3$, $HO_2\cdots(H_2O)_3a$, $HS\cdots(H_2O)_3$ and $HS\cdots(H_2O)_3a$ Complexes[a,b]

T/K	$H_2O\cdots HO_2$	$HO_2\cdots H_2O$	$HS\cdots H_2O$	$H_2O\cdots HS$	$H_2O\cdots H_2O$	$HO_2\cdots(H_2O)_2$	$HO_2\cdots(H_2O)_2a$
240	1.71E-17	6.19E-23	3.56E-22	1.68E-22	4.36E-22	2.01E-16	2.04E-16
250	9.32E-18	6.08E-23	3.16E-22	1.48E-22	3.34E-22	6.57E-17	6.65E-17
278	2.19E-18	5.91E-23	2.41E-22	1.10E-22	1.78E-22	4.41E-18	4.46E-18
288	1.40E-18	5.87E-23	2.23E-22	1.01E-22	1.47E-22	1.91E-18	1.93E-18
298	9.28E-18	5.83E-23	2.08E-22	9.36E-23	1.23E-22	8.76E-19	8.86E-19
298	(2.13E+09)[c]	(1.34E+04)[c]	(1.59E+02)[c]	(71.5)[c]	(7.18E+13)[c]	(1.90E+04)c	(1.90E+04)c
308	6.32E-18	5.82E-23	1.95E-22	8.74E-23	1.05E-22	4.23E-19	4.27E-19
325	3.48E-18	5.83E-23	1.77E-22	7.87E-23	8.15E-23	1.36E-19	1.38E-19
375	8.47E-18	5.97E-23	1.46E-22	6.28E-23	4.61E-23	8.92E-21	9.02E-21
425	2.97E-18	6.26E-23	1.30E-22	5.48E-23	3.09E-23	1.13E-21	1.14E-21

T/K	$HS\cdots(H_2O)_2$	$HS\cdots(H_2O)_2a$	$(H_2O)_3$	$HO_2\cdots(H_2O)_3$	$HO_2\cdots(H_2O)_3a$	$HS\cdots(H_2O)_3$	$HS\cdots(H_2O)_3a$
240	3.20E-22	4.84E-22	6.00E-20	7.84E-16	7.84E-16	3.92E-22	3.91E-22
250	2.09E-22	3.29E-22	2.95E-20	2.73E-16	2.73E-16	2.89E-22	2.88E-22
278	7.44E-23	1.31E-22	5.30E-21	2.14E-17	2.14E-17	1.40E-22	1.40E-22
288	5.41E-23	9.85E-23	3.12E-21	9.76E-18	9.76E-18	1.12E-22	1.12E-22
298	4.02E-23	7.58E-23	1.90E-21	4.70E-18	4.70E-18	9.16E-23	9.13E-23
298	(2.90E-03)c	(5.47E-03)c	(1.04E+11)[c]	(1.42E+00)c	(1.42E+00)c	(9.57E-06)[c]	(9.54E-06)c
308	3.04E-23	5.94E-23	1.20E-21	2.37E-18	2.37E-18	7.58E-23	7.56E-23
325	1.98E-23	4.08E-23	5.88E-22	8.20E-19	8.20E-19	5.68E-23	5.66E-23
375	7.04E-24	1.68E-23	1.06E-22	6.43E-20	6.43E-20	2.89E-23	2.88E-23
425	3.24E-24	8.77E-24	2.94E-23	9.40E-21	9.40E-21	1.78E-23	1.77E-23

[a] Equilibrium constants in units of $cm^3 \cdot molecule^{-1}$; [b] All equilibrium constants were calculated by using energies computed at CCSD(T)/6-311++G(3df,2pd) level and partition functions obtained at B3LYP/6-311+G(2df,2p) level; [c] The concentration of the corresponding complexes at 298 K

Table 2 Rate constants ($cm^3 \cdot molecules^{-1} \cdot s^{-1}$) for the $H_2S + {}^3O_2$ formations from the HO_2 + HS reaction without and with catalyst X ($X = H_2O$) within the temperature range of 240.0-425.0 K

T/K	k_{R1}	k_{RW1}	k_{RW2}	k_{RW3}	k_{RW4}
240	5.49E-11	5.44E-08	9.50E-09	6.38E-18	7.54E-14
250	4.98E-11	3.17E-08	7.97E-09	7.68E-18	7.26E-14
278	3.97E-11	9.22E-09	5.42E-09	1.25E-17	6.66E-14
288	3.72E-11	6.43E-09	4.86E-09	1.48E-17	6.51E-14
298	3.50E-11	4.65E-09	4.42E-09	1.73E-17	6.37E-14
308	3.32E-11	3.46E-09	4.07E-09	2.02E-17	6.26E-14
325	3.07E-11	2.23E-09	3.61E-09	2.60E-17	6.10E-14
375	2.60E-11	8.38E-10	2.83E-09	5.08E-17	5.84E-14
425	2.37E-11	4.36E-10	2.51E-09	9.05E-17	5.79E-14

k_{R1} is the rate constant of the $H_2S + {}^3O_2$ formations from the HO_2 + HS reaction without catalyst X (X=H_2O); k_{RW1}, k_{RW2}, k_{RW3}, and k_{RW4} is the rate constant of water-assisted the $H_2S + {}^3O_2$ formations from the HO_2 + HS reaction occurring through Channels RW1, RW2, RW3, and RW4, respectively.

Table 3 Effective rate constant ($cm^3 \cdot molecule^{-1} \cdot s^{-1}$) for water-assisted the $H_2S + {}^3O_2$ formations from the HO_2 + HS reaction within the temperature range of 240.0-425.0 K at different heights in the earth atmosphere

T/K	$[H_2O]$	k_{R1}	k'_{RW1}	k'_{RW2}	k'_{RW}	k_{tot}	k'_{RW1}/k_{tot}	k'_{RW2}/k_{tot}	k'_{RW}/k_{tot}
240	8.29E+15	5.49E-11	1.97E-13	4.87E-15	2.01E-13	5.51E-11	0.36%	0.01%	0.37%
250	2.21E+16	4.98E-11	2.34E-13	1.07E-14	2.45E-13	5.00E-11	0.47%	0.02%	0.49%
278	2.25E+17	3.97E-11	3.69E-13	7.20E-14	4.41E-13	4.01E-11	0.92%	0.18%	1.10%
288	4.25E+17	3.72E-11	4.02E-13	1.21E-13	5.23E-13	3.77E-11	1.07%	0.32%	1.39%
298	7.64E+17	3.50E-11	4.37E-13	1.97E-13	6.34E-13	3.56E-11	1.23%	0.55%	1.78%
308	1.31E+18	3.32E-11	4.76E-13	3.10E-13	7.86E-13	3.40E-11	1.40%	0.91%	2.31%
325	3.04E+18	3.07E-11	5.51E-13	6.40E-13	1.19E-12	3.19E-11	1.73%	2.01%	3.74%
375	2.12E+19	2.60E-11	8.19E-13	3.58E-12	4.40E-12	3.04E-11	2.69%	11.8%	14.47%
425	8.56E+19	2.37E-11	1.15E-12	1.34E-11	1.46E-11	3.83E-11	3.00%	35.0%	38.00%

k'_{RW1} and k'_{RW2} is the effective rate constant of water-assisted the $H_2S + {}^3O_2$ formations from the HO_2+ HS reaction occurring through Channels RW1 and RW2, respectively; $k'_{RW1}=k_{RW1} K_{eq}(H_2O\cdots HO_2)\,[H_2O]$, $k'_{RW2}=k_{RW2} K_{eq}(HO_2\cdots H_2O)\,[H_2O]$, $k'_{RW}=k'_{RW1}+k'_{RW2}$, $k_{tot}=k_{R1}+k'_{RW1}+k'_{RW2}$.

Table 4 Rate constants ($cm^3 \cdot molecules^{-1} \cdot s^{-1}$) and effective rate constants of the $H_2S + {}^3O_2$ formations from the HO_2+ HS reaction occurring through water dimer-assisted Channels RWW1-RWW3 and water trimer-assisted Channel RWWW1 within the temperature range of 240.0-425.0 K

T/K	k_{RWW1}	k_{RWW1a}	k_{RWW2}	k_{RWW2a}	k_{RWW3}	k_{RWW3a}	$[(H_2O)_2]$	k'_{RWW2}	k'_{RWW2a}	k_{RWWW1}	k_{RWWW1a}	$[(H_2O)_3]$	k'_{RWWW1}	k'_{RWWW1a}
240	2.63E-20	8.45E-20	7.26E-17	7.17E-17	4.01E-22	3.83E-22	3.00E+10	4.38E-22	4.38E-22	5.48E-18	7.31E-18	1.49E+07	6.40E-26	8.54E-26
250	5.14E-20	2.14E-19	9.01E-17	8.91E-17	4.60E-22	4.15E-22	1.63E+11	9.66E-22	9.65E-22	8.01E-18	2.10E-17	1.06E+08	2.32E-25	6.08E-25
278	3.32E-19	1.26E-18	1.56E-16	1.54E-16	7.75E-22	6.03E-22	8.99E+12	6.18E-21	6.18E-21	2.02E-17	3.57E-17	1.07E+10	4.63E-24	8.19E-24
288	9.76E-19	2.35E-18	1.86E-16	1.84E-16	9.68E-22	7.19E-22	2.65E+13	9.43E-21	9.43E-21	2.66E-17	4.78E-17	3.51E+10	9.12E-24	1.64E-23
298	1.92E-18	5.11E-18	2.21E-16	2.18E-16	1.23E-21	8.71E-22	7.18E+13	1.39E-20	1.39E-20	4.20E-17	7.05E-17	1.04E+11	2.05E-23	3.44E-23
308	4.22E-18	7.05E-18	2.60E-16	2.57E-16	1.58E-21	1.07E-21	1.79E+14	1.97E-20	1.96E-20	5.54E-17	9.78E-17	2.82E+11	3.71E-23	6.54E-23
325	8.27E-18	1.75E-17	3.37E-16	3.33E-16	2.45E-21	1.55E-21	7.54E+14	3.46E-20	3.46E-20	9.41E-17	1.90E-16	1.35E+12	1.04E-22	2.10E-22
375	9.32E-18	2.34E-17	6.59E-16	6.52E-16	9.26E-21	4.86E-21	2.07E+16	1.22E-19	1.22E-19	4.69E-16	7.11E-16	4.66E+13	1.40E-21	2.13E-21
425	5.21E-17	7.04E-17	1.16E-15	1.14E-15	3.24E-20	1.45E-20	2.26E+17	2.96E-19	2.96E-19	1.14E-15	2.43E-15	5.69E+14	6.10E-21	1.30E-20

k_{RWW1} and k_{RWW1a} is respectively the rate constant for the process of $HO_2 \bullet\bullet\bullet (H_2O)_2 + HS \rightarrow H_2S \bullet\bullet\bullet (H_2O)_2 + {}^3O_2$ and $HO_2 \bullet\bullet\bullet (H_2O)_2a + HS \rightarrow H_2S \bullet\bullet\bullet (H_2O)_2a + {}^3O_2$ in Channel RWW1; k_{RWW2} and k_{RWW2a} is respectively the rate constant for the process of $HO_2 \bullet\bullet\bullet (H_2O)_2 + HS \rightarrow H_2S \bullet\bullet\bullet (H_2O)_2 + {}^3O_2$ and $HO_2 \bullet\bullet\bullet (H_2O)_2a + HS \rightarrow H_2S \bullet\bullet\bullet (H_2O)_2a + {}^3O_2$ in Channel RWW2; k_{RWW3} and k_{RWW3a} is respectively the rate constant for the process of $HS \bullet\bullet\bullet (H_2O)_2 + HO_2 \rightarrow H_2S \bullet\bullet\bullet (H_2O)_2 + {}^3O_2$ and $HS \bullet\bullet\bullet (H_2O)_2a + HO_2 \rightarrow H_2S \bullet\bullet\bullet (H_2O)_2a + {}^3O_2$ in Channel RWW3; k_{RWWW1} and k_{RWWW1a} is respectively the rate constant for the process of $HO_2 \bullet\bullet\bullet (H_2O)_3 + HS \rightarrow H_2S \bullet\bullet\bullet (H_2O)_3 + {}^3O_2$ and $(HO_2 \bullet\bullet\bullet (H_2O)_3a + HS \rightarrow H_2S \bullet\bullet\bullet (H_2O)_3a + {}^3O_2$ in Channel RWWW1; $k'_{RWW2} = k_{RWW2} Keq(HO_2 \cdots (H_2O)_2) [(H_2O)_2]$; $k'_{RWW2a} = k_{RWW2a} Keq(HO_2 \cdots (H_2O)_2a)[(H_2O)_2])$; $k'_{RWWW1} = k_{RWWW1} Keq(HO_2 \cdots (H_2O)_3)[(H_2O)_3])$ $k'_{RWWW1} = k_{RWWW1a} Keq(HO_2 \cdots (H_2O)_3a)[(H_2O)_3]$.

Figure Caption

Fig. 1 Schematic energy diagrams of the channel of $H_2S + {}^3O_2$ formations from the HO_2 + HS reaction

Fig. 2 The optimized geometrical reactants for the HO_2+ HS reaction without and with catalyst X ($X = H_2O$, $(H_2O)_2$ and $(H_2O)_3$) at the B3LYP/6-311+G(2df,2p) level of theory

Fig. 3 Schematic energy diagrams of water-assisted the channel of $H_2S + {}^3O_2$ formations occurring through $H_2O\cdots HO_2$ + HS and $HO_2\cdots H_2O$ + HS

Fig. 4 Schematic energy diagrams of water-assisted the channel of $H_2S + {}^3O_2$ formations occurring through $HS\cdots H_2O$ + HO_2 and $H_2O\cdots HS + HO_2$

Fig. 5 Schematic energy diagrams of water dimer-assisted the channel of $H_2S + {}^3O_2$ formations occurring through $HO_2\cdots(H_2O)_2$ ($HO_2\cdots(H_2O)_2$a) + HS, $HS\cdots(H_2O)_2$ ($HS\cdots(H_2O)_2$a) + HO_2

Fig. 6 Schematic energy diagrams of water trimer-assisted the channel of $H_2S + {}^3O_2$ formations occurring through $HO_2\cdots(H_2O)_3$ ($HO_2\cdots(H_2O)_3$a) + HS

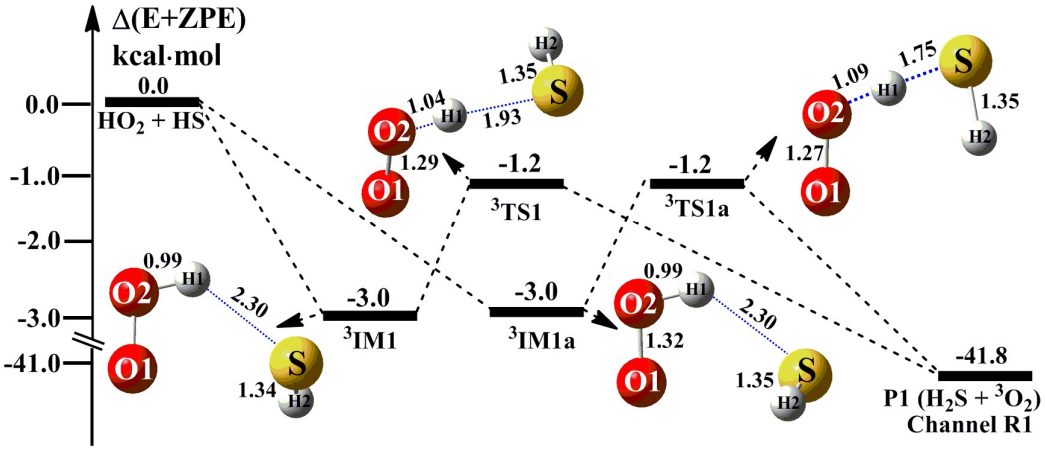

Fig. 1

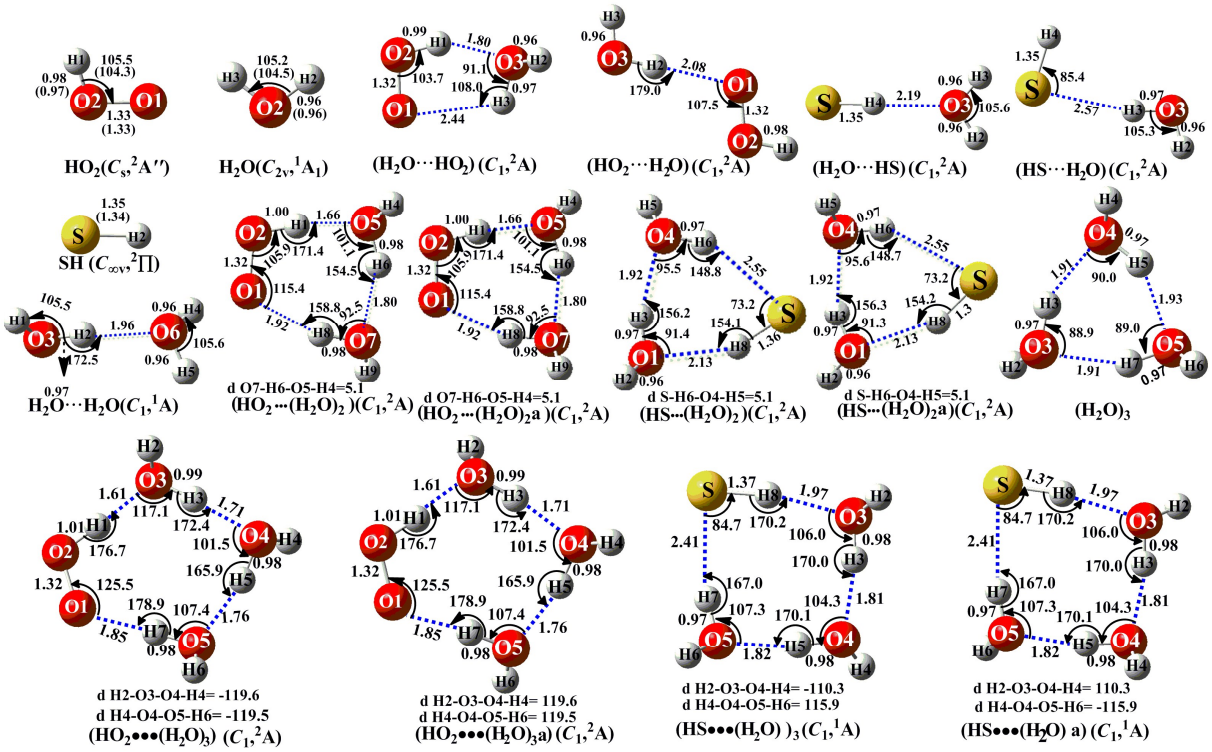

Fig. 2

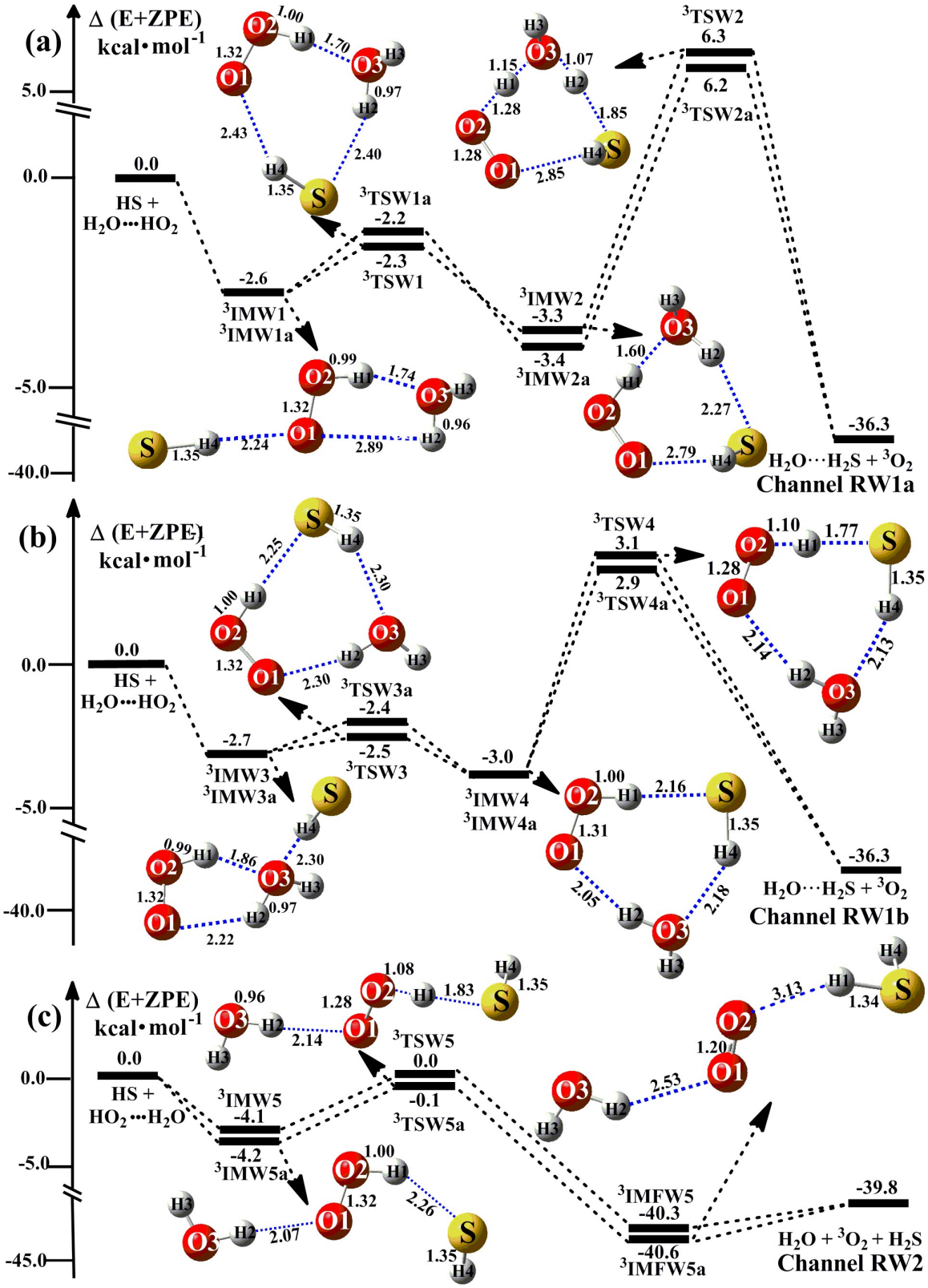

Fig. 3

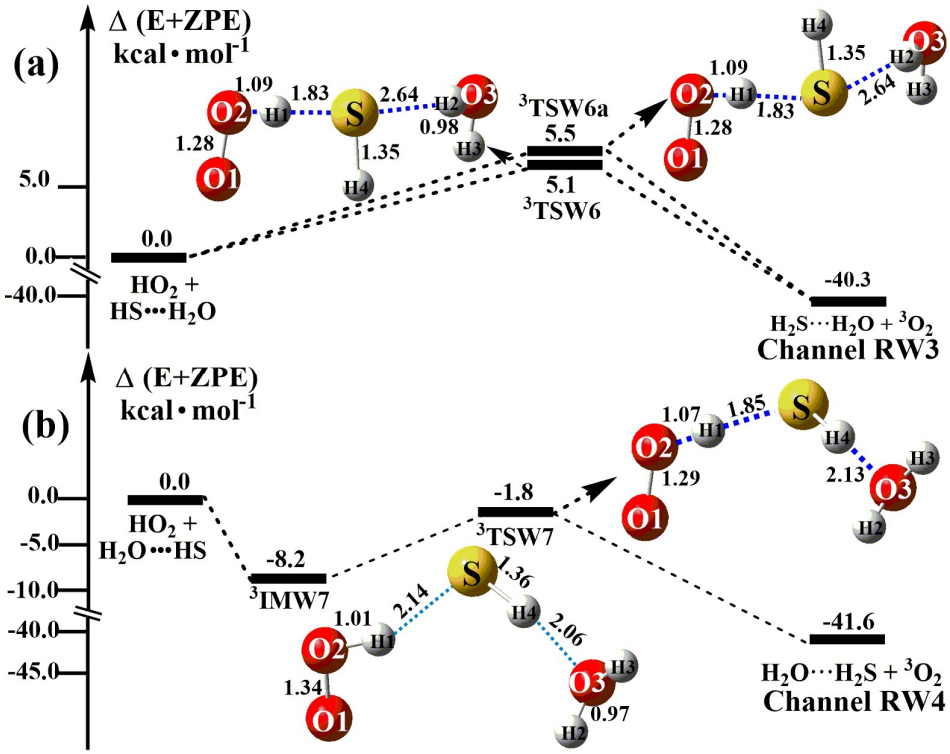

Fig. 4

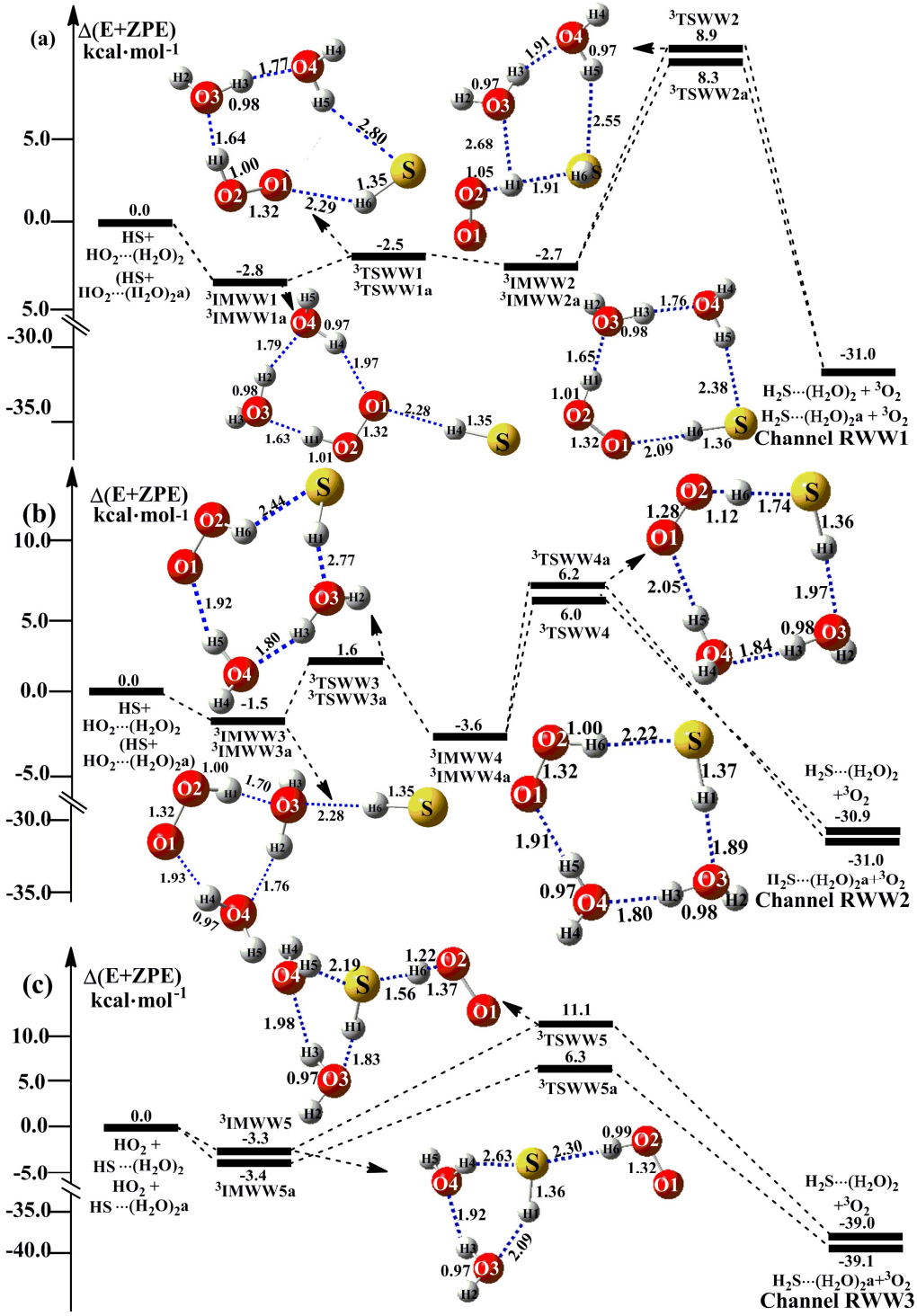

Fig. 5

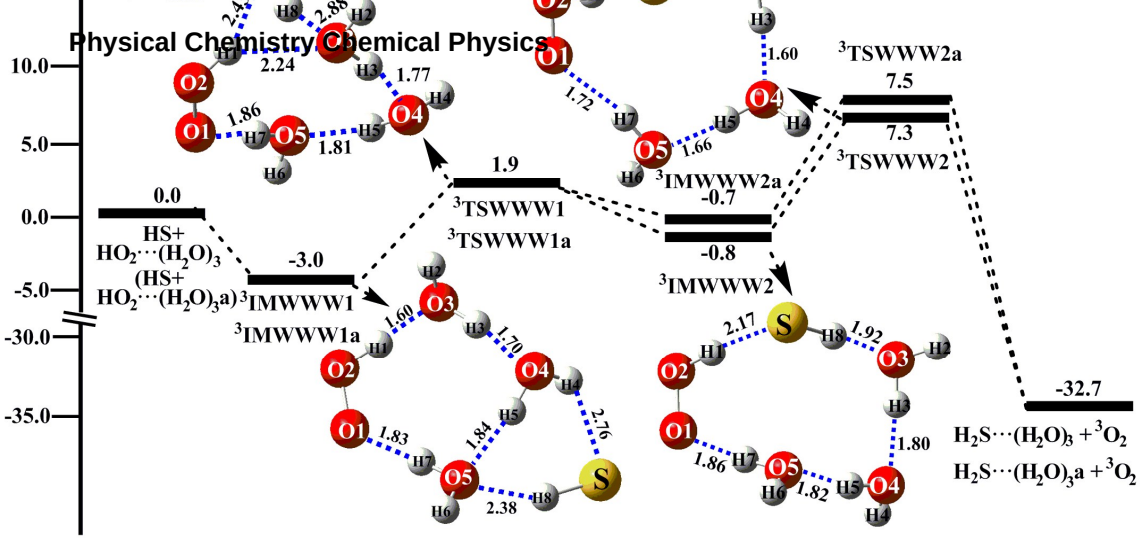

Fig. 6